2024 IEEE/RSJ International Conference on Intelligent Robots and Systems (IROS)
October 14-18, 2024. Abu Dhabi, UAE

Data-Driven Modeling of Ground Effect For UAV Landing on a Vertical Oscillating Platform

Binglin He, Heng Zhang, Baisheng Lai, Song Liu *Member, IEEE*, and Yang Wang* *Member, IEEE*

Abstract— **Landing on a vertically oscillating platform poses a significant challenge for multi-rotor unmanned aerial vehicle (UAVs) due to the time-varying ground effect (GE). In this work, we formulated a data-driven GE dynamic model that accurately describes the complex interactions between UAVs and both stationary and oscillating platforms. Integrating this model with a feedforward controller effectively compensates for GE, resulting in improved landing performance. The proposed GE model elucidates the relationship between GE and factors such as UAVs' velocity, throttle magnitude, and the motion of the landing platform. It highlights that the GE experienced during the landing process of UAVs is not only contingent on the current state but also related to past states. The resulting GE model is parsimonious and suitable for onboard computers with limited computational power, and its accuracy has been confirmed through a series of flight experiments. To demonstrate the effectiveness of the developed UAVs landing scheme, we compared our approach with robust control and internal model control methods. Experimental results indicate that the proposed landing strategy achieves faster and smoother landings, with at least a 22% improvement in smoothness and a 25% reduction in landing time.**

I. Introduction

UAVs play a crucial role in maritime missions, including search and rescue [1], survey missions [2], and environmental monitoring [3]. A key challenge in these scenarios is ensuring safe and quick landings on vessels. The nonlinear dynamics of UAVs, limited landing platform size, and the Ground Effect (GE), where rotor thrust increases near surfaces without additional power input [4], complicate this task. Additionally, landing on a vessel is further challenged by deck oscillations due to ocean waves, winds, and currents [5], which amplify the GE, potentially leading to instability or catastrophic failure [6, chapt.4]. Overcoming the influence of GE on an oscillating platform is thus vital for a smooth and fast UAV landing.

Existing solutions for addressing Ground Effect Force (GEF) fall into feedback and feedforward approaches. Feedback control (FBC) treats GEF as an external disturbance, using error signals to counteract it [5], [7]–[10]. However, this often results in delayed feedback [11] and challenges in achieving smooth, fast UAV landings. Feedforward control (FFC) predicts GEF using empirical formulas [12], [13] or neural networks (NN) [11] and incorporates compensation into pre-designed controllers. While effective, FFC relies heavily on the accuracy of GE prediction, which can be limited in complex scenarios like oscillating platforms. Data-driven models can account for additional factors but may suffer from increased complexity, overfitting, and a lack of interpretability. Moreover, existing GEF models typically do not consider the time evolution of GEF and are often based on stationary platform data, making them less accurate for predicting GEF during landings on oscillating platforms.

In this work, we aim to develop an accurate, reliable, and computationally efficient *dynamic* model of GEF for UAV landings on oscillating platforms, considering the states of both the UAV and the platform from the previous time step. Existing techniques like the Koopman operator [14], Dynamic Mode Decomposition (DMD) [15], and Sparse Identification of Nonlinear Dynamics (SINDy) [16] have all demonstrated certain success in identifying complex nonlinear dynamic models. Among them, SINDy stands out for its potential to achieve a fine balance between accuracy and complexity, preventing overfitting [16]. Hence, SINDy is chosen for this work as the core idea to derive our dynamic model of GEF. To ensure the accuracy of the GEF dynamic model developed through the SINDy methods, the effectiveness of the data and the correctness of the library functions are crucial. To achieve this, we establish a GEF data collection (DC) system to measure real-time GEF coupled with propeller thrust. Subsequently, we extract physics-informed knowledge from empirical formulas, and combine it with the higher-order terms and interaction terms of relevant variables we discovered, to form the library.

Finally, by combining GEF dynamic model with a feedforward controller, we succeed in achieving smooth and fast UAV landing on the vertically oscillating platform. A series of experiments confirm the accuracy of our GEF dynamic model, while our landing scheme for controlling UAV landing on the vertically oscillating platform has demonstrated superior smoothness and speed compared to using SSC and internal model-based control (IMBC) [17]. Our approach features two distinctive innovations: 1) The proposed GEF dynamic model is accurate and encompasses GEF and the state of both UAV and platform from previous time, facilitating UAV to achieve smooth and fast landing on vertically oscillating platforms. 2) We establish a GEF DC system that collects accurate data required for deriving GEF dynamic model and the model is parsimonious, ensuring successful implementation on UAV with limited computational power.

*Corresponding author
B. He, H. Zhang, S. Liu and Y. Wang are with the School of Information Science and Technology, ShanghaiTech University, Shanghai 201210, China (email: hebl2022, zhangheng1, liusong, wangyang4@shanghaitech.edu.cn)
B. Lai is with Alibaba Group, Shanghai 201210, China (e-mail: laibaisheng@gmail.com)

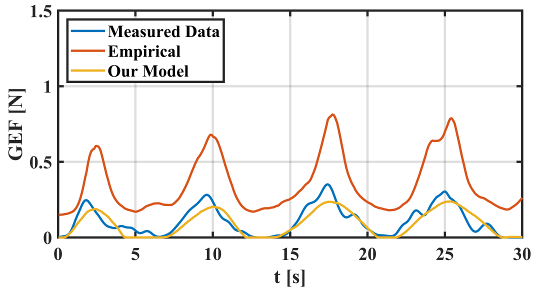

Fig. 1: GEF experienced by UAVs while the platform is **undergoing oscillating at a speed of 0.08 m/s** and T is set to $\mathbf{12}$ N.

II. Problem Statement

The dynamic model of the quadrotor considered in this work is standard [18]:

$$\dot{\mathbf{p}} = \mathbf{v}, \quad m\dot{\mathbf{v}} = m\mathbf{g} + R\mathbf{f}_u + \mathbf{f}_a \tag{1}$$

where $\mathbf{p} := [x_q,\ y_q,\ z_q]^\top \in \mathbb{R}^3$, $\mathbf{v} := [v_{x,q},\ v_{y,q},\ v_{z,q}]^\top \in \mathbb{R}^3$ represent the global position and velocity of the UAV, respectively. m is the mass of the UAV. $\mathbf{g} := [0,\ 0,\ g]^\top$ is the gravity vector, where g denotes the acceleration of gravity. $R \in \mathrm{SO}(3)$ is attitude rotation matrix. $\mathbf{f}_u := [0,\ 0,\ T]^\top$ denotes the total thrust from four propellers, $\mathbf{f}_a := [0,\ 0,\ f_{GEF}] \in \mathbb{R}^3$ denotes the residual aerodynamic force which is referred to as GEF[1].

Empirical GE models[2] [19] offer valuable insights into GE phenomena but are not accurate mainly due to their over-simplification. These models capture only the relationship between the current UAV state and the GEF, rather than the dynamics of GEF, leading to inaccuracies [20]. Moreover, they assume a stationary landing platform, making them unsuitable for moving platform scenarios. As shown in Fig. 1, it is evident that the GEF obtained from empirical formula (2) differs significantly from the measured GEF, whereas our proposed model achieves a more accurate estimation of measured GEF.

Therefore, this work aims to develop a data-driven model

$$\dot{\hat{f}}_{GEF} = \mathcal{F}(\hat{f}_{GEF}, \sigma, z, v_{z,q}, v_{z,p}) \tag{3}$$

for accurate GEF prediction during UAV landings, where throttle command σ, relative height z, Z-axis velocity of UAV $v_{z,q}$ and Z-axis velocity of the platform $v_{z,p}$ are considered. This model should retain the simplicity of empirical models, ensuring it can be applied to UAVs with limited computational power, unlike complex NN models.

[1]Note, the force $\mathbf{f}_a$ under consideration only accounts for its Z-axis component, while disregarding the forces in the other two directions. Because, although the platform may be oscillating vertically, the landing platform itself is horizontal.

[2]

$$\hat{f}^e_{GEF} = \frac{\mu\left(\frac{D}{8z}\right)^2}{1-\mu\left(\frac{D}{8z}\right)^2}T \tag{2}$$

where $T \in \mathbb{R}$ denotes the thrust generated by propellers in the absence of GE, $\hat{f}^e_{GEF} \in \mathbb{R}$ is the estimated GEF. $z \in \mathbb{R}$ is the relative height between the UAV and the platform. D is the rotor's diameter. μ is a constant coefficient depending on the number and arrangement of propellers.

III. Modeling and Landing Scheme Design

In this section, we detail the process of deriving a GEF dynamics model through data-driven approaches, followed by the design of a UAV landing scheme. The comprehensive modeling and landing scheme are depicted in Fig. 2.

A. SINDy [16].

Consider a nonlinear dynamical system of the form:

$$\frac{d}{dt}\mathbf{x} = f(\mathbf{x}, \mathbf{u}), \quad \mathbf{x}(0) = x_0 \tag{4}$$

with state $\mathbf{x} \in \mathbb{R}^n$, input $\mathbf{u} \in \mathbb{R}^q$ and dynamics $f(\mathbf{x}, \mathbf{u}) : \mathbb{R}^n \times \mathbb{R}^q \to \mathbb{R}^n$.

Given l snapshots of (4) measured over time, the system in (4) can be rewritten as

$$\dot{\mathbf{X}} = \mathbf{\Theta}(\mathbf{X}, \mathbf{U})\mathbf{\Xi} \tag{5}$$

where $\mathbf{\Theta}(\mathbf{X}, \mathbf{U})$ is the candidate library that is composed of linear and nonlinear functions of $\mathbf{X} = [x_1^\top, x_2^\top, \cdots, x_l^\top]^\top$ and $\mathbf{U} = [u_1^\top, u_2^\top, \cdots, u_l^\top]^\top$. $\mathbf{\Xi}$ is expected to be sparse by employing Sparse Relaxed Regularized Regression (SR3) [21] to identify the sparse matrix signifying the fewest nonlinearities in the library that result in a good model fit:

$$\begin{aligned}\xi_k =& \underset{\hat{\xi}_k}{\operatorname{argmin}} \frac{1}{2}\left\|\dot{\mathbf{X}}_k - \mathbf{\Theta}(\mathbf{X}, \mathbf{U})\hat{\xi}_k\right\|_2^2 + \\ & \lambda\left\|w\right\|_0 + \frac{1}{2\nu}\|\hat{\xi}_k - w\|_2^2, \quad k = 1, ..., l\end{aligned} \tag{6}$$

where $\dot{\mathbf{X}}_k$ is the k-th row of $\dot{\mathbf{X}}$, ξ_k is the k-th row of Ξ, and λ is the sparsity-promoting hyperparameter. $\|\cdot\|_2$ and $\|\cdot\|_0$ represent the l_2 norm and the l_0 norm of the matrices or vectors respectively. $\|\cdot\|_0$ promotes sparsity in the auxiliary variable w which is forced to be close to $\hat{\xi}_k$ corresponding estimate of ξ_k, although it is not convex. ν is a relaxation parameter that controls the gap between $\hat{\xi}_k$ and w.

B. GEF DC System

To obtain precise UAV thrust data, we've developed a GEF DC system, as shown in Fig.3, comprising a UAV, a six-axis force sensor, and a movable landing platform. This setup enables direct real-time thrust measurement and manipulation of the force (f_{GEF}) between the UAV and the platform. The structure of the GEF DC system can be outlined as follows:

(1) **UAV** is fixed $\mathbf{0.75}$ m above the platform.
(2) **The six-axis force sensor** with a precision of $\mathbf{0.1}$ g and a weighing range of up to $\mathbf{20}$ kg is installed at the connection point between the UAV and the 2 degree-of-freedom motion ring to measure the thrust data.
(3) **Oscillating platform** used to simulate a UAV landing surface consists of a square plane with side length of $\mathbf{1.5}$ m and three electric actuators. The platform is capable of operating smoothly without any impact with a load of up to $\mathbf{100}$ kg.
(4) **Data acquisition card** serves as the data acquisition unit for the system and transmits real-time thrust data to the PC via WiFi at a frequency of $\mathbf{100}$ Hz.

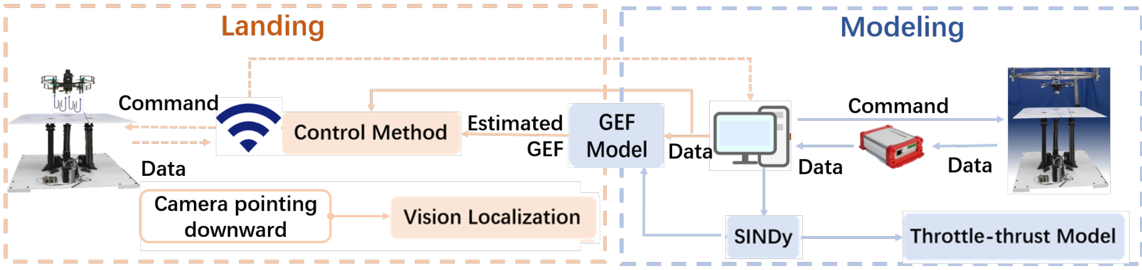

Fig. 2: UAV landing block diagram, including modeling of GEF and the design of the landing scheme. The part within **the blue box** represents the construction of the GEF dynamics model using SINDy. The part within **the orange box** illustrates the UAV landing on a vertically oscillating platform under the proposed landing scheme.

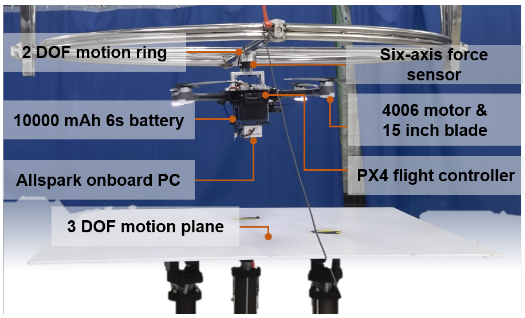

Fig. 3: Schematic of the GEF DC System

C. Modeling of Throttle-Thrust and f_{GEF}

a) Throttle-Thrust Model: For the extraction of f_{GEF} from the total thrust data, first, a throttle-thrust model is essential. In view of a fundamental observation in [22, ch.6.1], the thrust dynamic formula can be derived as follows:

$$\dot{T}_{sr} = \frac{c_0\sigma + c_1 - T_{sr}}{T_{\mathrm{m}}} \tag{7}$$

we denote the square root of T as $T_{sr} \in \mathbb{R}$, and c_0, c_1, T_m are the constants. In (7), the SINDy library's variables were defined, but empirical formulas typically neglect higher-order and interaction terms. Through iterative selection, an optimized library was identified to enhance the SINDy model's predictive accuracy.

$$\mathbf{\Theta_T} := \{1, T_{sr}, \sigma, \sigma^2, T_{sr}^3, \exp(-T_{sr})\sigma, \sin(T_{sr})\sigma\}$$

Following a procedure similar to Section III-A, we employed sparse regression to identify a small subset of active terms from the library $\mathbf{\Theta_T}$. In this way, the model $\mathcal{T}(\cdot)$ that relates throttle to thrust can be written in the following form:

$$\dot{\hat{T}}_{sr} = \mathcal{T}(\hat{T}_{sr}, \sigma) = \mathbf{\Theta_T \Xi_T} \tag{8}$$

where $\hat{T}_{sr} \in \mathbb{R}$ represents the estimated T_{sr}. $\mathbf{\Xi_T}$ is the expected sparse matrix of coefficients identified by employing SR3. This throttle-thrust model can achieve a real-time estimation of T, the given initial thrust value and σ.

b) GEF Model: With the estimation of thrust, we can extract the real-time f_{GEF} from the measured thrust data obtained from the GEF DC system. In Eq. (2), the relationship between f_{GEF}, T, and z is established for a stationary platform. Yet, our focus on UAV landings on oscillating platforms presents new complexities. The varying relative distance and velocity between the UAV and platform lead to a fluctuating GEF that a static equation cannot accurately represent. A dynamic GEF model is necessary to address these challenges. Inspired by above observations, the SINDy library $\mathbf{\Theta_{GEF}}$ is selected as follows:

$$\mathbf{\Theta_{GEF}} := \{1, f_{GEF}, \sigma, z, v_{z,q}, v_{z,p}, \sigma^2, z^2, v_{z,q}^2, v_{z,p}^2\}$$

Following a procedure similar to (8), the GEF dynamic model admits the following form

$$\dot{\hat{f}}_{GEF} = \mathcal{F}(\hat{f}_{GEF}, \sigma, z, v_{z,q}, v_{z,p}) = \mathbf{\Theta_{GEF}\Xi_{GEF}} \tag{9}$$

where $\mathbf{\Xi_{GEF}}$ is expected sparse matrix of coefficients. The point to be explained here is that $v_{z,q} = a_{z,q}t + v_{0z,q}$, in which $a_{z,q} = (f_u + f_a - mg)/m \in \mathbb{R}$ and $v_{0z,q} \in \mathbb{R}$ denotes the given initial velocity of UAV in Z-axis direction. $v_{z,p}$ is calculated by subtracting v_z from $v_{z,q}$.

D. UAV Landing Control Method Based on GEF Model

The paper's objective is to enhance UAV landing performance via feedforward the estimation the GEF into a nonlinear feedback control method [11]. Define the position tracking error $\tilde{\mathbf{p}} := \mathbf{p} - \mathbf{p}_d$ with the desired position $\mathbf{p_d} \in \mathbb{R}^3$, and a composite variable $\mathbf{s} \in \mathbb{R}^3$,

$$\mathbf{s} = \dot{\tilde{\mathbf{p}}} + \Gamma\tilde{\mathbf{p}} = \dot{\mathbf{p}} - \mathbf{v}_r$$

where Γ is a positive definite matrix and $\mathbf{v_r} \in \mathbb{R}^3$ is the reference velocity. It is worth noting that when $\mathbf{s}$ exponentially converges to a region around $\mathbf{0} \in \mathbb{R}^3$, $\mathbf{p}$ will exponentially converge to the vicinity of the desired trajectory $\mathbf{p}_d(t)$ [23].

The proposed controller can be formulated as:

$$\mathbf{f}_u = m\dot{\mathbf{v}}_r - K_P\mathbf{s} - K_I\int \mathbf{s}dt - m\mathbf{g} - \hat{\mathbf{f}}_a \tag{10}$$

with positive constants K_P and K_I, and feedforward term $\hat{\mathbf{f}}_a = [0, 0, \hat{f}_{GEF}]^\top$.

Substituting Eq. (10) into Eq. (1), the closed-loop dynamics is rewritten as $m\dot{\mathbf{s}} + K_P\mathbf{s} + K_I\int \mathbf{s}dt = \boldsymbol{\epsilon}$, with the estimated error $\boldsymbol{\epsilon} := \mathbf{f}_a - \hat{\mathbf{f}}_a \in \mathbb{R}^3$. Consequently, $\tilde{\mathbf{p}}(t)$ will converge globally and exponentially to a bounded residual region with respect to $\|\epsilon\|$ [24].

IV. Experimental Results

To affirm the proposed landing scheme's viability, we conducted four experiments: real-time throttle-thrust and GEF model estimation, and autonomous UAV landings on both ground and oscillating platforms. The second and third experiments highlight the models' and scheme's efficiency for swift and stable landings in various conditions.

In our experiments, we used a quadcopter UAV weighing 1.37 kg with a Jetson Xavier NX onboard Linux computer.

Communication with PX4 was established via Robot Operating System (ROS) using MAVROS messages over WiFi at a frequency of 100 Hz. To achieve more precise landings, we also employed AprilTag for localization in the XY plane.

A. Data Collecting and Modeling

To derive the throttle-thrust model, we controlled the UAV using various throttle signals, i.e. five sets of ramp signals with different slopes within the range of 0.2 to 0.8, as well as five sets of sine signals with an amplitude of 0.8 and different frequencies.

These thrust data are considered sufficient to derive the model as they encompass the complete range of throttle signals that the UAVs may encounter in diverse scenarios.

Additionally, to establish an accurate model, it is essential to have reliable, and low-noise data. Therefore, we first conducted enough repeated trials to collect valid data, and we applied a Savitzky-Golay filter with an appropriate window length to smooth the data, ensuring that the trend was preserved without altering the data's width. Based on the processed data, the throttle-thrust model was derived utilizing SINDy method as follows:

$$\begin{aligned}\dot{\hat{T}}_{sr} &= 0.215 - 0.650\hat{T}_{sr} + 13.882\sigma \\ &+ 11.815\sigma^2 - 0.123\hat{T}_{sr}^3 - 12.825\sigma^3 \\ &- 16.647\exp(-\hat{T}_{sr})\sigma - 1.457\sin(\hat{T}_{sr})\sigma\end{aligned} \tag{11}$$

Then, the estimated thrust $\hat{T}$ can be calculated from $\hat{T} = \hat{T}_{sr}^2$. By subtracting the real-time measured thrust from $\hat{T}$, the real-time f_{GEF} at each moment can be obtained. Additionally, to establish a universal GEF dynamic model, three scenarios were designed to collect more comprehensive data.

(1) σ remains **constant** while the platform is **undergoing oscillating at a speed of 0.08 m/s**.
(2) σ is set to a **sinusoidal signal** while the platform remains **stationary**.
(3) σ is set to a **sinusoidal signal** while the platform is **undergoing oscillating at a speed of 0.08 m/s**.

Similar to process (11), GEF dynamic model is derived:

$$\begin{aligned}\dot{\hat{f}}_{GEF} &= 0.804 - 0.088\hat{f}_{GEF} - 3.912\sigma \\ &+ 0.586z + 1.051v_{z,p} - 1.049v_{z,q} \\ &+ 4.854\sigma^2 + 1.103v_{z,p}v_{z,q} - 2.504z^2 \\ &- 0.535v_{z,p}^2 - 0.562v_{z,q}^2\end{aligned} \tag{12}$$

B. Validation of Throttle-thrust and GEF Dynamic Model

1) Validation of throttle-thrust model In the experiment, we validated the accuracy of the throttle-thrust model (11). Initially, we set σ to increase gradually from 0.2 to 0.3. Subsequently, after achieving thrust stability, we adjust σ according to $\sigma = 0.1(t-10)$. We observed real-time T and $\hat{T}$, along with the corresponding estimated error, as depicted in Fig. 4(a) and (b).

Then, we set the throttle σ from 0.2 to 0.3 initially and then started to perform a sinusoidal motion $\sigma = \sin(0.8(t-10))$. The result is displayed in Fig. 4(c) and (d). Those results show that within a certain range of throttle variations

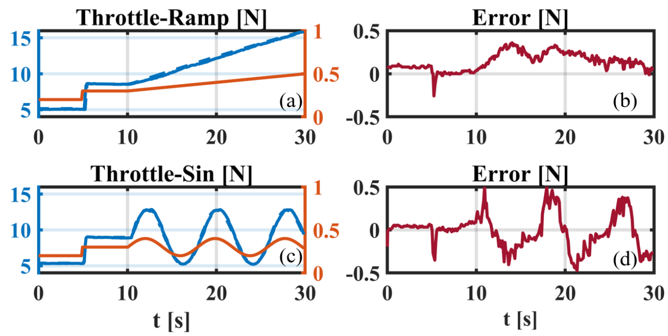

Fig. 4: Experimental results of **throttle-thrust model** estimation when σ is set to **(a)** a ramp signal and **(c)** a sinusoidal signal. **(b)(d)** show the corresponding estimate errors of **(a)(c)** between T and $\hat{T}$. The **blue solid and dotted lines** denote the **real-time** T and $\hat{T}$ respectively, and **orange solid line** denotes the σ. These figures demonstrate that the **trottle-thrust model** is **sufficiently accurate**.

σ, our model consistently achieves a precise thrust estimation with small deviations.

2) Validation of GEF dynamic model In this part, we conducted two sets of experiments where the platform moves in two modes: gradually approaching the UAV and oscillating at a speed of 0.08 m/s. Additionally, both experiments comprised six individual trials, each lasting 30 seconds.

In each trial, UAV is set to generate an initial thrust of $10N$, $11N$, $12N$, $13N$, $14N$, $15N$, and $16N$ respectively, while remaining the throttle command unchanged. These experiments are conducted to demonstrate the effectiveness of the GEF model (12) in various scenarios.

Fig. 5(a)(b) depicts the curves of real-time f_{GEF} and $\hat{f}_{GEF}$ for both experiments. According to Fig. 5(a), we can conclude that as the platform gradually approaches the UAV, our GEF mode (12) exhibits small errors and quickly tracks the actual f_{GEF}. In Fig. 5(b), compared to the previous experiment, the average error and variance have increased, indicating that (12) experiences some errors when there is a fast change in the relative distance between the UAV and the platform. However, the mean absolute errors across different thrust levels remain within $0.2N$ and have minimal impact on the landing.

C. Comparative Experiments of UAV Landing on Ground

In this subsection, we evaluate three landing schemes for UAV ground landing to showcase the effectiveness of our approach. Method I utilizes nonlinear feedback control. Method II enhances this with a feedforward component derived from an empirical GEF formula. Method III, our method, introduces a control law (10) for improved landing performance.

In all our experiments, we set the same controller parameters: K_p is set to 4, K_I to 0.01, and Γ to 2. The UAV begins its descent from a certain height above the platform. Taking into account the height of the landing gear, the UAV is considered to have landed when it reaches a height of 0.1 m above the ground. The reference trajectory $z_r(t)$ for the UAV is given by

$$z_r(t) := e^{-Ct}(1+Ct)(z_{init} - h_d) + h_d \tag{13}$$

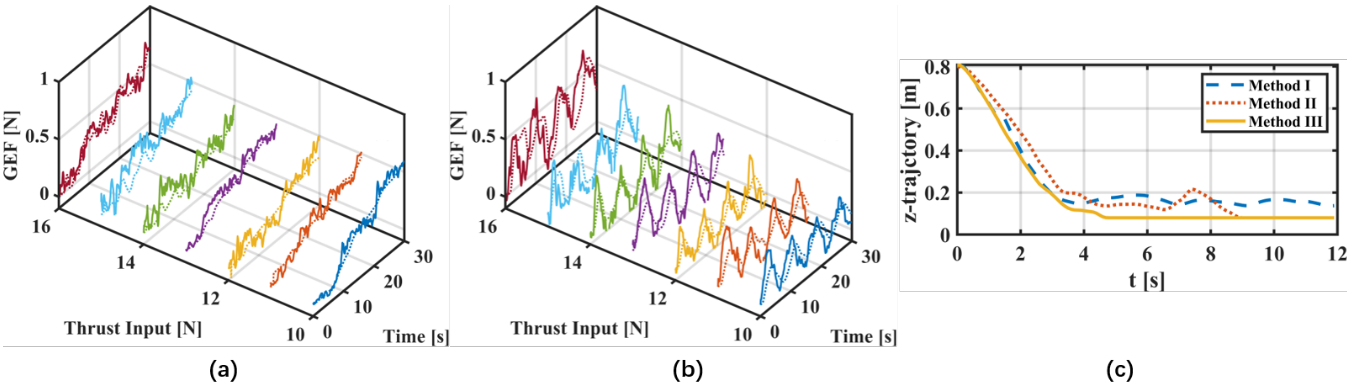

Fig. 5: Our **GEF dynamic model** accurately estimates f_{GEF} when the platform **(a)** gradually approaches UAV **(b)** continues to oscillate. Errors in **(b)** increase compared to **(a)**, but it remains within a small range. **Colors solid and dotted lines** represent the **real-time** f_{GEF} and $\hat{f}_{GEF}$ calculated by **GEF model** respectively. **(c)** Z-axis trajectory of UAV landing on the ground with three different methods.

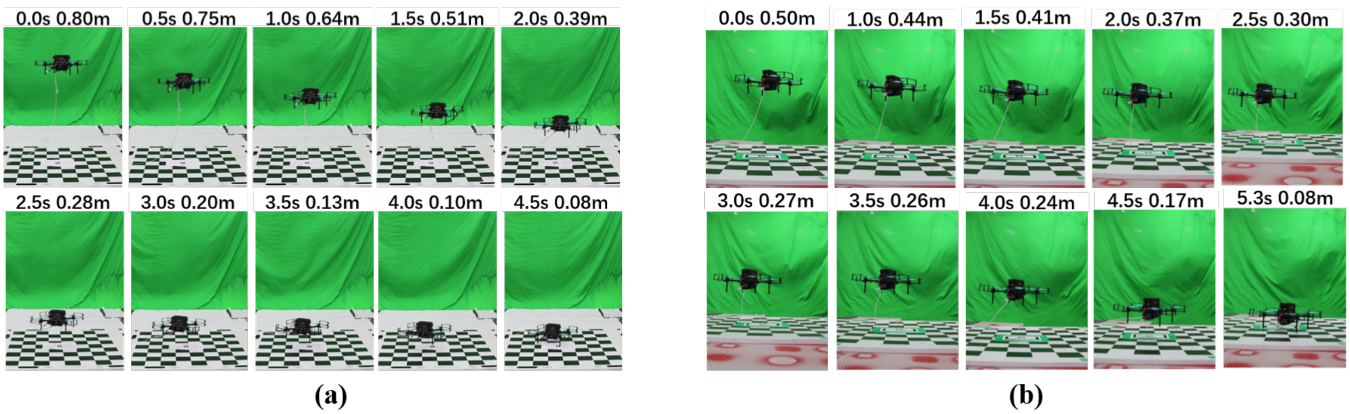

Fig. 6: The successive stages of UAV landing on **(a)** ground **(b)** the vertically oscillating platform. In both cases, UAV all successfully achieved fast and smooth landing. These illustrations confirm the efficacy of our landing scheme.

where $C = 0.1$ is related to the landing velocity, $z_{init} = 0.8$ and h_d refer to the initial height and desired height of the UAV relative to the landing platform, respectively. In this experiment and the experiment in IV-D, we require the UAV to complete the landing, thus setting h_d to 0.0 m.

In Fig. 5(c), experiments show the UAV hovers about 15 cm above the ground without compensation, taking an average of 7.1 s to land using empirical GEF formulas. Our proposed scheme significantly reduces landing time to an average of 5.1 s over 5 trials, offering a faster and smoother landing. The detailed landing process is illustrated in Fig. 6(a).

D. Comparative Experiments of UAV Landing on the Vertical Oscillating Platform

In this part, the vertically oscillating platform moves in a sinusoidal motion mode with an amplitude of 0.05 meters and a frequency of 0.5 Hz.

Three control methods were employed for comparative experiments: internal model-based control (IMBC) [17], smooth sliding control (SSC) [5], and our method (10). Each control method should perform the UAV landing on the vertically oscillating platform experiment five times, starting from $z_{init} = 0.5$ m, to ensure the validity of the experimental results.

Experimental data were collected and analyzed based on the landing time T_L, the landing velocity V_L, which is the relative velocity between the UAV and the landing platform at the landing point, and the total variation S_L of the landing trajectory L. The formula for calculating the total variation is as follows:

$$S_L(L) = \int_0^{T_L} |\dot{L}(t)| dt$$

where $\dot{L}(t)$ is the velocity of the landing trajectory $L(t)$ at time instant t. $S_L(L)$ represents the smoothness of L, with smaller values indicating smoother curves.

Table I presents the average values of the three metrics mentioned above. From the table, it is evident that our method control the UAV to land in the shortest time, completing the descent approximately 25% faster than the other two methods. The landing speed at the touchdown point is also the lowest, being only around 50% of the speeds associated with the other two methods. Moreover, the descent curve is the smoothest, being 78% of the smoothness of the SSC method and 54% of the IMBC method. These results demonstrate the effectiveness of the proposed modeling and landing scheme. From Fig. 6(b) and Fig. 7, it is also evident that the proposed landing scheme enables fast and smooth UAV landings on the vertically oscillating platform.

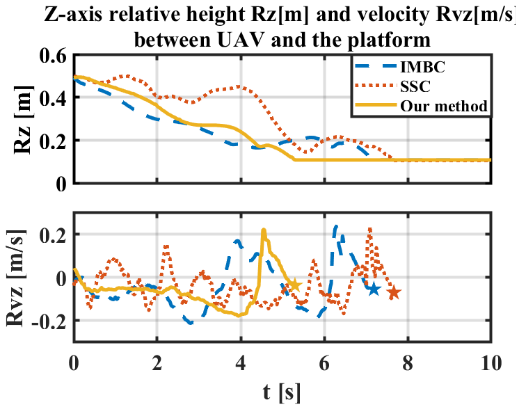

Fig. 7: Z-axis relative height and relative velocity between UAV and the vertically oscillating platform. **Blue, orange and yellow pentagram** denote the velocity of the UAV relative to the platform at the final stage of landing.

TABLE I: Performance Metrics of UAV Landing on the Vertical Oscillating Platform

Method	$\mathbf{T_L}$[s]	$\mathbf{V_L}$[m/s]	$\mathbf{S_L}$
IMBC	7.46	0.086	23.69
SSC	7.69	0.084	16.52
Our method	**5.38**	**0.036**	**12.89**

V. CONCLUSION

This paper introduces an efficient and precise GEF dynamic model using the SINDy method, integrated as a feedforward term into a nonlinear feedback control strategy for UAV landing on vertically oscillating platforms. A GEF data collection platform is also developed to obtain real-time thrust data, aiding in the modeling of throttle-thrust and GEF, with the latter extracted from the measured data in real-time. The GEF model is notable for its sparsity and interpretability, facilitating stability analysis with various control methods and suitable for UAVs with limited computational resources. Extensive real-world experiments confirm the proposed landing scheme's effectiveness, including UAV landings on both the ground and oscillating platforms, and validate the model's accuracy. Looking ahead, we plan to refine the GEF model with advanced SINDy techniques to account for additional platform states like tilt angles and terrain. We also aim to integrate this model with more specialized control schemes to further enhance UAV landing performance on oscillating platforms.

REFERENCES

[1] B. Kiefer and A. Zell, "Fast region of interest proposals on maritime uavs," in *2023 IEEE International Conference on Robotics and Automation (ICRA)*, 2023, pp. 3317–3324.

[2] L. Gonçalves and B. Damas, "Automatic detection of rescue targets in maritime search and rescue missions using uavs," in *2022 International Conference on Unmanned Aircraft Systems (ICUAS)*, 2022, pp. 1638–1643.

[3] J. Jessin, C. Heinzlef, N. Long, and D. Serre, "A systematic review of uavs for island coastal environment and risk monitoring: Towards a resilience assessment," *Drones*, vol. 7, no. 3, p. 206, 2023.

[4] A. Matus-Vargas, G. Rodriguez-Gomez, and J. Martinez-Carranza, "Ground effect on rotorcraft unmanned aerial vehicles: A review," *Intelligent Service Robotics*, vol. 14, no. 1, pp. 99–118, 2021.

[5] A. J. Peixoto, D. Pereira-Dias, and R. H. R. Andrade, "Smooth robust control applied to quadrotor landing," in *2019 IEEE 58th Conference on Decision and Control (CDC)*, 2019, pp. 7875–7880.

[6] C. Powers, D. Mellinger, A. Kushleyev, B. Kothmann, and V. Kumar, "Influence of aerodynamics and proximity effects in quadrotor flight," in *Experimental Robotics: The 13th International Symposium on Experimental Robotics*. Springer, 2013, pp. 289–302.

[7] Y. Zou and K. Xia, "Robust fault-tolerant control for underactuated takeoff and landing uavs," *IEEE Transactions on Aerospace and Electronic Systems*, vol. 56, no. 5, pp. 3545–3555, 2020.

[8] P. Wei, S. N. Chan, S. Lee, and Z. Kong, "Mitigating ground effect on mini quadcopters with model reference adaptive control," *International Journal of Intelligent Robotics and Applications*, vol. 3, pp. 283–297, 2019.

[9] J. Díaz-Téllez, J. F. Guerrero-Castellanos, F. Pouthier, N. Marchand, and S. Durand, "In-ground-effect disturbance-rejection altitude control for multi-rotor uavs," *Journal of Intelligent & Robotic Systems*, vol. 109, no. 2, p. 27, 2023.

[10] T. H. Anh, N. T. Binh, and J. W. Song, "In-ground-effect model based adaptive altitude control of rotorcraft unmanned aerial vehicles," *IEEE Robotics and Automation Letters*, vol. 7, no. 2, pp. 794–801, 2022.

[11] G. Shi, X. Shi, M. O'Connell, R. Yu, and K. Azizzadenesheli, "Neural lander: Stable drone landing control using learned dynamics," 2018.

[12] B. Hu, L. Lu, and S. Mishra, "Fast, safe and precise landing of a quadrotor on an oscillating platform," in *2015 American Control Conference (ACC)*. IEEE, 2015, pp. 3836–3841.

[13] L. Danjun, Z. Yan, S. Zongying, and L. Geng, "Autonomous landing of quadrotor based on ground effect modelling," in *2015 34th Chinese Control Conference (CCC)*, 2015, pp. 5647–5652.

[14] C. Folkestad, D. Pastor, and J. W. Burdick, "Episodic koopman learning of nonlinear robot dynamics with application to fast multirotor landing," in *2020 IEEE International Conference on Robotics and Automation (ICRA)*. IEEE, 2020, pp. 9216–9222.

[15] J. N. Kutz, S. L. Brunton, B. W. Brunton, and J. L. Proctor, *Dynamic mode decomposition: data-driven modeling of complex systems*. SIAM, 2016.

[16] S. L. Brunton, J. L. Proctor, and J. N. Kutz, "Discovering governing equations from data by sparse identification of nonlinear dynamical systems," *Proceedings of the National Academy of Sciences*, vol. 113, no. 15, pp. 3932–3937, 2016.

[17] L. Marconi, A. Isidori, and A. Serrani, "Autonomous vertical landing on an oscillating platform: an internal-model based approach," *Automatica*, vol. 38, no. 1, pp. 21–32, 2002.

[18] A. Paris, B. T. Lopez, and J. P. How, "Dynamic landing of an autonomous quadrotor on a moving platform in turbulent wind conditions," in *2020 IEEE International Conference on Robotics and Automation (ICRA)*, 2020, pp. 9577–9583.

[19] I. Cheeseman and W. Bennett, "The effect of ground on a helicopter rotor in forward flight. 1955," *ARC R&M*, no. 3021.

[20] X. Kan, J. Thomas, H. Teng, H. G. Tanner, V. Kumar, and K. Karydis, "Analysis of ground effect for small-scale uavs in forward flight," *IEEE Robotics and Automation Letters*, vol. 4, no. 4, pp. 3860–3867, 2019.

[21] K. Champion, P. Zheng, A. Y. Aravkin, S. L. Brunton, and J. N. Kutz, "A unified sparse optimization framework to learn parsimonious physics-informed models from data," *IEEE Access*, vol. 8, pp. 169 259–169 271, 2020.

[22] Q. Quan, *Introduction to multicopter design and control*. Springer, 2017.

[23] M. O'Connell, G. Shi, X. Shi, K. Azizzadenesheli, A. Anandkumar, Y. Yue, and S.-J. Chung, "Neural-fly enables rapid learning for agile flight in strong winds," *Science Robotics*, vol. 7, no. 66, p. eabm6597, 2022.

[24] X. Shi, K. Kim, S. Rahili, and S.-J. Chung, "Nonlinear control of autonomous flying cars with wings and distributed electric propulsion," in *2018 IEEE Conference on Decision and Control (CDC)*. IEEE, 2018, pp. 5326–5333.